Original Paper

Buried Pipe Detection Under the Road by High Resolution Frequency Domain GPR

Shanker Man SHRESTHA*1, Yoshiyuki TOMIZAWA*2 and Ikuo ARAI*3

Abstract

In this paper, ground-penetrating radar (GPR), which has the capability to do non-destructive testing (NDT) in civil engineering field, is proposed to detect underground gas pipes, water pipes, electric cables or voids under a road. SFCW (Stepped Frequency Continuous Wave) radar, which is based on vector network analyzer, is utilized for target detection and its performance is investigated. Since signal processing is vital for targets reorganization and clutter rejection, we categories the signal processing method into two phases. In first phase, the numbers of the frequency domain radar data traces underwent CPM (Combined Processing Method) to obtain two dimensional time domain data. In second phase, the two-dimensional time domain data was processed by SAR (Synthetic Aperture Radar) method to obtain the three dimensional image of the pipes. The field experiment was performed on a gravel road with an asphalt layer at a road construction company's test site in Saitama-shi, Japan and all the signal-processing results are presented.

Keywords : GPR, SFCW Radar, FFT, MUSIC Algorithm, SAR,Super Resolution Signal & Image Processing.

1. Introduction

The detection of buried pipes and cables has been a challenging issue for the construction and maintenance of road. In addition, characterizing underground surface at the construction site for the study of bearing capacity of soil, measuring the thickness of a roadway's pavement layer are the major topics of interest in the field of civil engineering[1]. However, there are several limitations such as existence of natural clutter such as metallic can, nails, and stone in the environment. Non-homogeneity of soil is also a burning problem, which alter a relative permittivity of the soil and makes the scenario complicated to characterize the underground surface[2)~8)]. Nevertheless, ground-penetrating radar (GPR) has been well-established and mature technology for the non-destructive testing (NDT) in civil engineering field and widely applied in overcoming such problems. Most GPR are in the time domain using the pulse signal, and sensitivity and maximal detectable depth are usually limited by the size of antenna and the dielectric constant of the soil. Recently, more FMCW (Frequency Modulation Continuous Wave) GPRs are emerging due to larger dynamic range, less power consumption, and more convenient calibration. Unlike to conventional impulse type radar, which has been studied over years, the SFCW (Step Frequency Continuous Wave) radar has attractive features such as capable of operating with high central- frequency over the ranges of several gigahertz, large dynamic range, and higher computation facilities and so on. In this paper, we applied the SFCW radar to detect underground gas pipes, water pipes, electric cables or voids buried under a road[2)~5) 9)]

Signal processing is vital for target reorganization and clutter rejection in GPR. GPR normally required high resolution to get the clear information of the physical and geometrical characteristic of the buried targets[4]. Basically, there are two ways to improve the resolution, which are vertical resolution and azimuth resolution. The vertical resolution can be achieved by inverse filter such as Weiner filter, Gaussian method and so on and a super resolution technique such as MUSIC (Multiple Signal Classifications)[10)~15)], MEM (Maximum Entropy Method)[16)], ESPRIT (Estimation of Signal Parameter via Rotation Invariance Technique)[17)]. The azimuth resolution can be achieved by holograph Image Processing Method, and Migration Technique (Synthetic Aperture Radar Processing)[18)~20)]. In this paper, we implement the MUSIC algorithm to improve the vertical resolution. In addition, we use CPM (Combined Processing Method)[4], which is a method of combining the time domain results of

(Received November 6, 2006. Accepted January 9, 2008)

*1 Schlumberger K.K., 2–2–1 Fuchinobe, Sagamihara-shi, Kanagawa 229–0006, Japan

*2 Department of Electric Media Technology, Gunma National College of Technology, 580 Toriba-machi, Maebashi-shi, Gunma 370–8530, Japan

*3 1–48–31 Funabashi, Setagaya-ku, Tokyo 156–0055, Japan

Fig. 1 S parameters S_{11} measurement of bow-tie antenna by vector network analyzer.

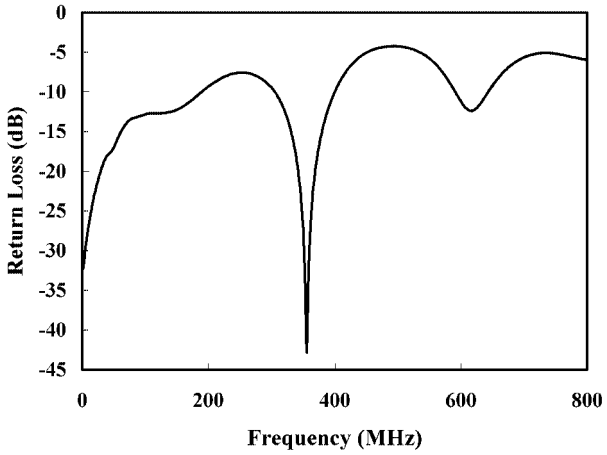

Fig. 2 Measured input loss versus frequency.

MUSIC and IFFT (Inverse Fast Fourier Transform) to achieve a good tradeoff between high resolution and a high precision signal level. Finally, we use SAR (Synthetic Aperture Radar) processing method to improve the azimuth resolution and also to reconstruct the three dimensional images.

2. SFCW Radar System

The SFCW radar produces the synthetic pulse that sweeps through a pre-defined frequency band, which increases in step wise, and measures the return signal strength at different frequencies to obtain the frequency spectrum of the target return. The major components involve in this research are as following.

1. Antenna System
2. Vector Network Analyzer
3. Signal processing unit

2.1 Antenna System

Antennas are a very important parts of GPR equipment. The main requirement for a good GPR antenna is wide bandwidth. Element antennas such as dipole and bow tie antennas (usually resistive loaded) are considered as broadband antenna. The waves radiated from the antenna are attenuated, but the cost is loss of efficiency[21]. The directivity function of a GPR antenna is also vital, which depends upon the dielectric properties of the surveyed half space and the distance from it[22]. In order to satisfy the bandwidth requirement, element antennas like shielded (ferrite covered) bow-tie antennas, which has been developed at the University of Electro-Communications, Tokyo is applied in this research work. The shield prevents interference from the spurious signal or echoes coming from the environment and improves the directivity of the antenna. The antennas were resistively loaded and the dimension of the antenna was ($40\times25\times10$) cubic centimeter.

In order to check the performance of the antenna, the frequency domain measurement has been done using the vector network analyzer (See Fig. 1), which has capability to take a measurement from 30 kHz to 40 GHz and a selected numbers of frequency points are 201, 401, 801 and 1601. The bandwidth was selected 800 MHz (0 MHz to 800 MHz) and a selected number of frequency was 801. The return loss of an antenna was measured and the measured return loss versus frequency is shown in Fig. 2. The reflection coefficient was found less than -30 dB for the range 100 MHz to 500 MHz. Thus, the performance of the antenna is good within this bandwidth range.

2.2 Vector Network Analyzer

The commercial vector network analyzer works as a SFCW radar[14]. The commercial vector network analyzer (Agilent 8712ET RF) was used for the measurement campaign. The Vector Network Analyzers optimized for production measurements of reflection and transmission parameters. The instrument integrates an RF synthesizer sources, transmission/reflection test set, multi-mode receivers, and display in compact box. The frequency band ranges from 300 kHz to 1300 MHz and a selected number of points (frequencies) are 201, 401, and 801. The three-channel, dual mode receivers provide dynamic range of greater than 100 dB in narrow band direction measurement mode, which is also the interest of this experiment. The receiver incorporates digital signal processing and microprocessor control for fast operation and measurement throughput. The major advantage of vector network analyzer (SFCW radar) system stems from the potential for controlling an ultra wideband around the central frequency for a given application and for obtaining a higher dynamic range.

2.3 Signal Processing Unit

A lap top computer is a signal-processing unit, which is shown in Fig. 3. The receiving signal from the RF output of the vector network analyzer is stored in the computer. The acquisition from the network analyzer to the computer is done

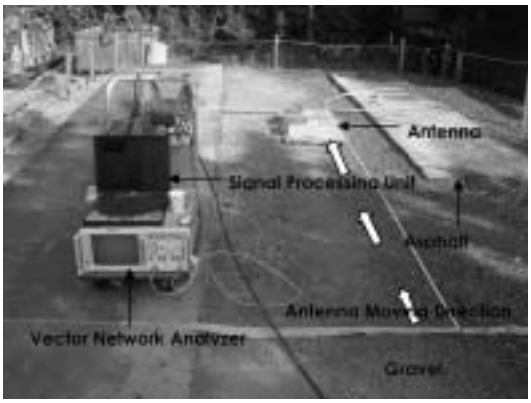

Fig. 3 A SFCW radar system components such as antennas, vector network analyzer, and signal processing unit. This system is used for measurement campaign both on the asphalt and gravel to detect the water pipes, gas pipes and ducts buried under the road pavement.

by "GPIB-USB A" cable (National Instrument). The software used for data acquisition is developed in Visual Basic. Since the vector network analyzer is used, the data acquisition process is in frequency domain and the signals are coherent signals. This frequency domain signals having extremely high dynamic range are processed by proposed signal processing algorithm. The authors have developed the entire signal processing software-using MATLAB.

3. Signal Processing Approach

This research deals with a signal processing method used to increase the vertical and azimuth resolution of a radar image and to obtain a high precision signal level. As mentioned above, we used SFCW radar, which is based on vector network analyzer. This SFCW radar operates in the frequency domain and is almost similar to the FMCW radar except the frequency changes in steps. The vector network analyzer transmits the frequency domain signal and received the complex reflected signal at different frequencies. This reflected frequency domain data is considered as a radar signal[23].

Since signal processing is vital for target detection and clutter rejection, we categories the signal processing method into two phases. In first phase, The frequency domain radar signal spectrum undergoes IFFT and MUSIC processing simultaneously to obtain a high precision receiving signal level and high resolution signal respectively. Time domain responses are obtained in both cases. The time domain response of IFFT and MUSIC[24)~28)] are combined, in a process we call CPM as shown in Fig. 4. The numbers of the frequency domain radar data traces underwent CPM and the results were arranged in an array to obtain two dimensional time

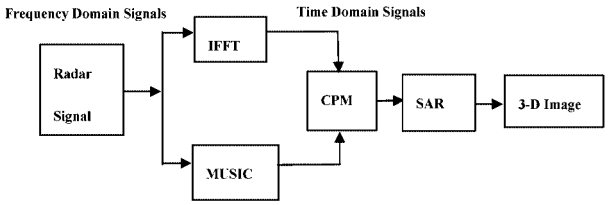

Fig. 4 Simple block diagram of radar signal processing approach.

domain data. In second phase, the two-dimensional time domain data was processed by SAR method and image is presented as shown in Fig. 4. The theoretical concepts of the signal-processing algorithm applied in this research work are briefly explained as following.

3.1 MUSIC Algorithm

The MUltiple SIgnal Classification (MUSIC) algorithm is a nonparametric spectral estimation technique, which estimates multiple scattering centers from the observed voltage received on an array of antenna utilizing the eigenvector. The eigenvectors can be used to compute a spectrum with TOA (Time of arrival)[5) 7) 8)], i.e., estimate delay time of high frequency spectrum[11)]. The Eigen value of diagonal matrix helps to estimate the numbers of reflected signals.

The measured value of reflected signal from the target with a vector network analyzer can be expressed using vector notation as follows.

$$\boldsymbol{x}=\boldsymbol{A}\boldsymbol{y}+\boldsymbol{w} \tag{1}$$

where,

$$\boldsymbol{x}\cong[x_1,\ x_2\cdots\cdots x_L]^{\mathrm{T}} \tag{1a}$$

$$\boldsymbol{A}\cong[\boldsymbol{a}(\tau_1),\ \boldsymbol{a}(\tau_2)\cdots\cdots\boldsymbol{a}(\tau_k)] \tag{1b}$$

$$\boldsymbol{a}(\tau_k)\cong[\mathrm{e}^{-j2\pi f_1\tau_k},\mathrm{e}^{-j2\pi f_2\tau_k}\cdots\cdots\mathrm{e}^{-j2\pi f_L\tau_k}]^{\mathrm{T}} \tag{1c}$$

$$\boldsymbol{y}\cong[y_1,\ y_2\cdots y_k]^{\mathrm{T}} \tag{1d}$$

$$\boldsymbol{w}\cong[w_1,\ w_2\cdots w_k]^{\mathrm{T}} \tag{1e}$$

Here, T represents transpose. Again $\boldsymbol{a}(\tau)$ vector can be declared by its time and it is called a mode vector. $\boldsymbol{A}$ is a delay parameter matrix, which has L numbers of arrays and the k^{th} element of row. Therefore, L can be regarded as the number of signals. $\boldsymbol{y}$ is the reflection coefficient of the L^{th} reflection point at frequency f_L, *and* $\boldsymbol{w}$ is a noise vector.

The position (delay time) of each reflection point can be estimated by searching the peak position of the MUSIC function (P_{music})

$$P_{music}(\tau)=\frac{\boldsymbol{a}(\tau)^*\boldsymbol{a}(\tau)}{\boldsymbol{a}(\tau)^*\boldsymbol{E}_N\boldsymbol{E}_N^*\boldsymbol{a}(\tau)} \tag{2}$$

where, $\boldsymbol{a}(\tau)$ is a delay time mode vector and $\boldsymbol{E}_N$ is noise L (L

$-k$) matrix whose columns are the ($L-k$) noise eigenvector.

Ground Penetrating Radar signals are generally coherent signals as the measurements was taken by SFCW radar based on vector network analyzer. The vector network analyzer generates the identical signal, and the phase and the amplitude of the reflected signals also do not change from snap shot to snap shot. MUSIC fails to work properly when the signals are coherent. So, a decorrelation process or specifically speaking Spatial Smoothing Process (SSP)[13] is performed in order to eliminate the problems encountered with coherent signals. The received signal is divided into the numbers of overlapping sub arrays or snap shots. Consequently, the phase is changed in each snap shot. The spatially smoothed covariance matrix is defined as the sample means of the sub array covariance and expressed as

$$S_{SSP}=\frac{1}{M}\sum_{k=1}^{M}S_k \tag{3}$$

3.2 CPM (Combined Processing Method)

CPM is a method of combining the time domain results of MUSIC and IFFT to achieve a good tradeoff between high resolution and a high precision signal level[4]. Let the complex IFFT results in the time domain be represented by $X(t)$ and the MUSIC results in time domain is represented by $Y(t)$. The time domain results of IFFT and MUSIC are combined using the Combined Processing Method (CPM), which is calculated using the following expression.

$$Z(t)=\frac{X\left|\frac{\partial Y}{\partial t}\right|+Y\left|\frac{\partial X}{\partial t}\right|}{\sqrt{\left|\frac{\partial Y}{\partial t}\right|^2+\left|\frac{\partial X}{\partial t}\right|^2}} \tag{4}$$

where, $Z(t)$ is the time domain data of CPM.

In order to explain the equation (4), mathematical analysis has been performed. Since combining the time domain responses of IFFT and MUSIC are performed by calculating the slope and the position of the signal, the delay of IFFT response signal and MUSIC response signal should be coincided, which is a required condition. So, in this particular condition, when we consider the point at the peak (centre) of the curve (Fig. 5), the slope of MUSIC will be very higher than the slope of IFFT due to sharp response of MUSIC. This can be expressed mathematically by

$$\frac{\partial Y}{\partial t}>>\frac{\partial X}{\partial t} \text{ so that } \frac{\partial X}{\partial t}\geq 0$$

Substituting the value of $\frac{\partial X}{\partial t}$ in Eq. (4) gives

$$Z(t)=X \tag{4a}$$

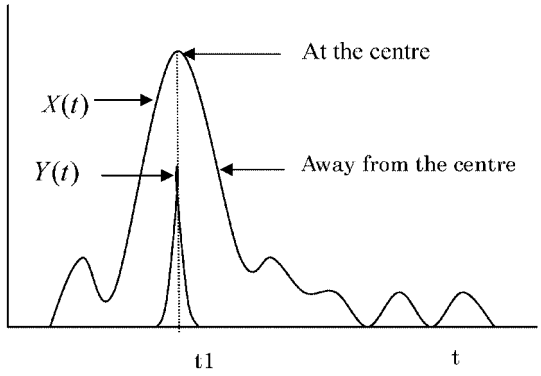

Fig. 5 IFFT and MUSIC response curve to demonstrate the CPM method.

The Eq. (4a) means the signal level of $Z(t)$ will be the amplitude of the IFFT. Similarly, when we consider the point drifted from the peak (center) of the curve (Fig. 5), the slope of IFFT response curve is very higher than MUSIC response curve. It can also be expressed mathematically by

$$\frac{\partial X}{\partial t}>>\frac{\partial Y}{\partial t} \text{ so that } \frac{\partial Y}{\partial t}\geq 0$$

Substituting the value of $\frac{\partial Y}{\partial t}$ in Eq. (4) gives

$$Z(t)=\mathrm{Y} \tag{4b}$$

The Eq. (4b) means the signal level of $Z(t)$ will be the amplitude of the MUSIC. Therefore, it is found that $Z(t)$ selects the precision signal level of X (IFFT response) when the slope of X is low and also select the signal level of Y (MUSIC response) when the slope of Y is low.

3.3 SAR processing

In SAR processing[18)~20) 23)], a set of transmitting and receiving antennas are seperated equally over a synthetic aperature length. This is also known as migration technique[19) 20)]. The time domain radar signal is received, which can be represented in the A-scope and the B-scope. The echoes from the point target are represented in the A-scope as shown in Fig. 6. When the co-ordinates of the point target are $P(x_i, y_j)$, the echoes or receiving signal are distributed along a trajectory, which is expressed as following

$$y^2=(x-x_i)^2+y_j^2 \tag{5}$$

The echo received at the antenna, which is just above the point target is higher than the echo received at the antenna which is away from the point target. All the distributed echoes along the trajectory are combined to get high signal level at (x_i, y_j), which is expressed as

$$Q(x_i, y_j)=\sum_{m=-M}^{M}D_m.\,P(x_{i+m}, y_m) \tag{6}$$

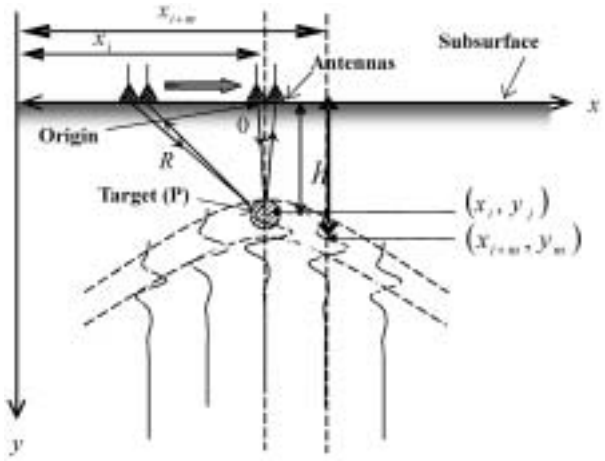

Fig. 6 SAR processing method (Migration technique).

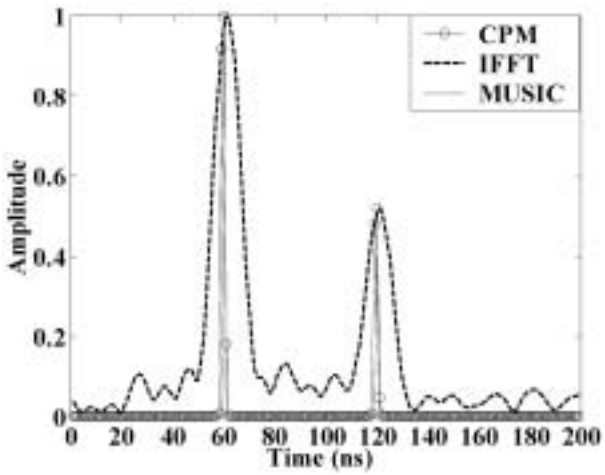

Fig. 7 MUSIC, IFFT and CPM response from the frequency domain signal Simulated signal is a sinusoidal wave with frequency bandwidth = 200 MHz, sampling point = 200, Sampling frequency = 1 MHz.

Where $y_m = \sqrt{(x_{i+m} - x_i)^2 + y_j^2}$ and D_m is weighting function. *Normally, the* $D_m = 1$ for soil because the attenuation is high. $2M+1$ is the total number of echoes along the trajectory. If an ideal impulse is transmitted and received, the horizontal (azimuth) resolution received by the Eq. (4) would be equal to $2M+1$ antenna being spaced over a synthetic aperture length.

4. Computer Simulations

The main objectives of the simulation are to examine the resolution, precision of amplitude, and computation speed of CPM. In order to meet this objective we generated the frequency domain sinusoidal wave using the following formula.

$$x = \sin\omega_1 + \sin\omega_2 \tag{7}$$

The sampling frequency was set to be 1 MHz and sampling number was set to be 200. Therefore, the bandwidth was 200 MHz. The delay time was set to be 60 ns and 120 ns, which generate the two signals. It is expressed by the following equations.

$$d = e^{-j\omega\tau_1} + 0.5e^{-j\omega\tau_2} \tag{8}$$

The second signal was set to the half of the first signal in order to check the amplitude level of CPM response. The frequency domain signal thus generated was processed by MUSIC, IFFT and CPM method and the results are shown in Fig. 7. From the simulations result (Fig. 7), it is found that the resolution of MUSIC is very high, and it is the most attractive feature of MUSIC algorithm. However, we could observe the amplitude of second signal less than half of the first one, which is supposed to be half according to its setting. In contrast to this, FFT response shows the amplitude of the second signal half of the first one but resolution is sharply declined and also loss of energy in the form of side lobes. CPM has high precision signal level than MUSIC and very high resolution than FFT at the small expenses of SNR.

Computation time is also an important achievement of CPM because CPM uses the information of FFT and the computation time of FFT is very fast. The computation time of MUSIC is long due to the eigen-value calculation, which is documented in most of the signal processing. It is also stated that the precise amplitude of the signal could be calculated from by MUSIC processing. This could be possible if the signal covariance matrix and noise covariance matrix is calculated to get the eigenvalues and its corresponding eigen vectors. The eigen decomposition the of the signal coveriance matrix can be expressed as following.

$$\begin{aligned} S &= xx^* \\ &= (Ay + w)(Ay + w)^* \end{aligned} \tag{9}$$

where, * denotes complex conjugate transpose.

$$S = Ay(Ay)^* + w^*(Ay) + w(Ay)^* + ww^* \tag{10}$$

Since $w^*(AY)$ & $w(Ay)$ are zero, then

$$S = Ayy^*A^* + ww^* \tag{11}$$

Hence $yy^* = P$ is diagonal matrix, then the signal coverance Matrix can be written as

$$S \cong APA^* + \sigma^2 I \tag{12}$$

Where P is the signal covariance matrix and σ^2 is the noise power in each channel. The eigenvalue of this array covariance matrix and the corresponding eigenvectors gives the information such as number of signal and time of arrival

(delay time), which is calculated using Peak MUSIC (PMUSIC). Spatial Smoothing Process (SSP) is performed as a pre-processing method to decorrelate the coherent signal. If the frequency domain array with L reflection coefficient that extend from (1,2,3$\cdots N$, $N+1,\cdots L$-1,L), making M number of overlapping snap shots having length N, then the relation between L, M and N can be written as

$$M=L-N+1 \tag{13}$$

The computation time of the MUSIC can be decrease by increasing the value of M. As the value M is increased, N will be decreased, since L is a constant term for certain frequency domain signal. This will reduce the size of covariance matrix and the computation time will also fast. In this simulation, L was set to be 250. When the value of M was set 10, the size of signal covariance matrix become (239×239) resulting the computation time becomes very long. However, the precision signal amplitude is high and stable. In contract, when the M was set to be 230, the size covariance matrix become (29×29), which is very small and the computation time reduces by 10 times. However, we could not get correct amplitude. So, in order to achieve the high speed computation, we increased the number of snap shot and just estimate the peak position of MUSIC function and combined with IFFT result to get correct amplitude. Thus high speed, high resolution and correct amplitude is achieved. This algorithm is perfectly fit to perform signal and image processing of GPR data.

5. Experiments on a Road

5.1 Experiment Setup

The primary objective of the research work is to detect the water pipes, gas pipes, cables or duct under the road layer, which is important to detect before construction and maintenance of the road. Therefore, the resulting experimental setup used for the work described in the paper is summarized in Fig. 3. It is a test site of a road construction company in Saitama-shi, Japan, which is design to test the performance of GPR. The test site was 8 meters long and 4 meters width. Various types of pipes and voids are buried as in normal road in the town. The asphalt layer was about 4 cm thick. The experimental field was an inhomogeneous type composed of asphalt, gravel and soil. We used the migration technique, which is not sensitive to the dielectric constant of the soil[20]. So, the average dielectric constant value was set to be 10. The measurement was taken both on the surface of the gravel and the asphalt layer.

In order to derive the dielectric constant 10, the following expression can be written.

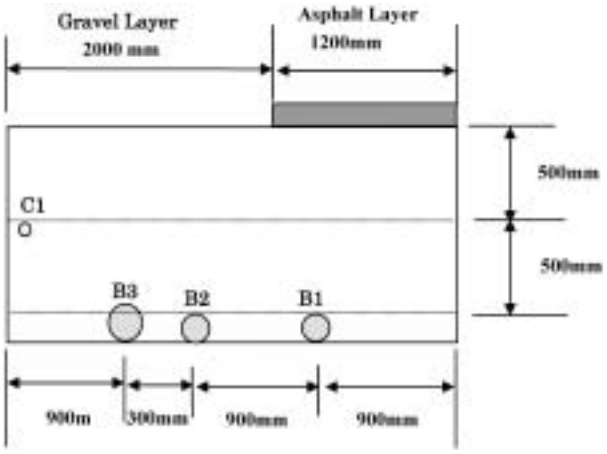

Fig. 8 Geometry of the pipes buried below the ground surface.

Table 1 Material, Diameter and Depth of the Pipes.

Pipe Symbol	Material	Diameter	Depth
B1	PLV (Vinyl Chloride)	50 mm	1m
B2	Steel	50 mm	1m
B3	Steel	100 mm	1m
C1	PLV	13 mm	0.5 m

$$R=\frac{\tau c}{2\sqrt{\varepsilon_r}} \tag{14}$$

where,

τ : delay time

c : velocity of light

ε_r : relative permittivity of the medium

The depth of the target is known value 1 meter and delay time was recorded about 21 ns. If we substitute these values in equation (14), we will obtain the relative permittivity 10.

5.2 Data Acquisition for Experiment

The antenna was moved at the increment of 10 cm up to 3.2 meters in x-axis on the surface of the gravel and the asphalt to scan the underground targets (See Fig. 3). Several such scan were taken in y-axis at the increments of 10 centimeters shift. The geometry of the targets is shown in Fig. 8. The pipe material, depth, and its diameters are presented in Table 1. SFCW radar was used for the measurement campaign. The principal advantages of SFCW radar over a conventional GPR are high dynamic range, and the wide range of frequency band application, which can be varied at the different site on a required basis. In this measurement, the frequency band selected was 600 MHz (1 MHz-601 MHz). Within the limit of 600 MHz frequency band, the effective bandwidth utilized during signal processing was 400 MHz (100 MHz to 500 MHz) because the return loss of the antenna was found less than −10 dB from 100 MHz to 500 MHz, which is found from Fig. 2. The detail parameter setting for the vector

Table 2 Parameter setting for field experiment.

Frequency Band	600MHz (1-601) MHz
No. of Points	401
Sweep time	80 ms
Small change in frequency	1.5 MHz
Soil Permittivity ε_r	10
Test Site	Inhomogeneous medium
Radar Type	SFCW radar

network analyzer and experiment are shown in Table 2.

5.3 Signal Processing Results

In this measurement, the total scanned length was 3.2 m and the first 2 m was gravel road and the later 1.2 m was asphalt road. The raw data received from the measurement is shown in Fig. 9, when the radar antennas were above the target B2 (Steel pipe with 50 mm diameter). This frequency domain data having real and imaginary information underwent conversion by the IFFT algorithm, and MUSIC algorithm and the results are shown in Fig. 9 (b). The time domain results were obtained in both cases. It is found from this experimental result that the IFFT response has precise signal level, however the resolution is poor. In contrast, MUSIC response has very high resolution but the received signal level from the target is higher than the coupling signal level, which is practically not acceptable and it means that the precision of receiving signal level of MUSIC is insufficient. Therefore, the CPM processing method was performed combining time domain response of IFFT and CPM, which is also shown in Fig. 9 (b). The CPM response has higher resolution than IFFT and highly précised amplitude than MUSIC response.

The B-scan image processed by IFFT, MUSIC, and CPM is shown in Plate 1 (a), (b), and (c) respectively. The results in Plate 1 are presented in linear scale. The value of color bar is the intensity of signal level, in other words, it's discrimination between the targets, clutters, and the surroundings. If the results are closely visualized, image reconstruction of target B 2 and target B3 is clearly seen in image processed by MUSIC and CPM. However, the image processed by IFFT doesn't demonstrate the sharp image reconstruction of target B2 and target B3 due to its low-resolution characteristic. The time side lobe effect is also prominent in IFFT response. The reflected signal from the target B1 is very weak as it is a PLV (Vinyl chloride) pipe with diameter 50 mm. Accordingly, the image of target B1 is also weak and ambiguous. As the test site is an inhomogeneous field mixed with stone, the reflection from stone and clutter is also observed in IFFT, MUSIC, and CPM results. The upper portion of the image is due to the effect of direct coupling, which is shown in the B-scan image, processed by CPM (see Plate 1 (c)). The coupling (direct wave) between the transmitting antenna and the receiving

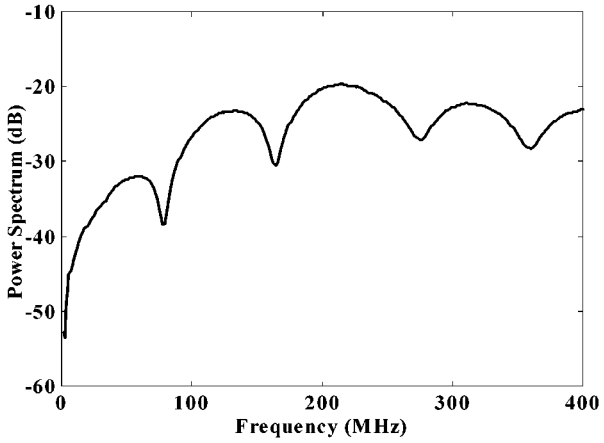

Fig. 9 (a) Frequency domain radar spectrum measured on the gravel and asphalt.

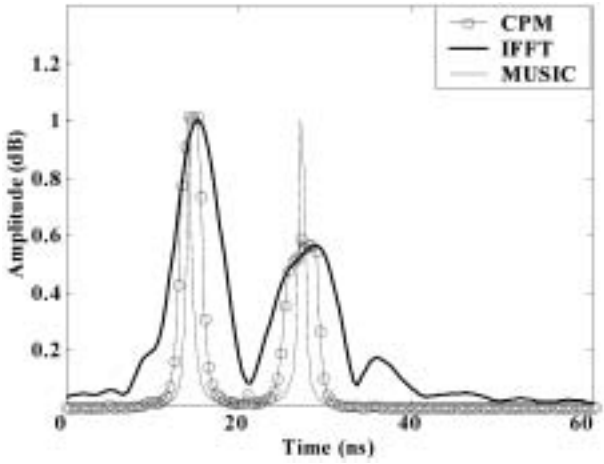

Fig. 9 (b) Experimental results to demonstrate the IFFT, MUSIC, and CPM responses (Bandwidth = 600 MHz, frequency point = 401, frequency interval = 1.5 MHz).

antenna, and the coupling between the antenna and the ground surface is known as the "directing coupling". The effect caused by this direct coupling is termed as coupling effect. This coupling effect can be visualized in the B-scan image processed by IFFT and MUSIC. The data was measured on the surface of the asphalt and its effect is sharply seen in the B-scan of MUSIC response (see Plate 1 (b)).

It is found from the experiment that the result obtained on the gravel layer is better than the result obtained on the asphalt layer because signal reflected from the asphalt layer is higher than the signal reflected from the gravel layer. In this experiment campaign, the antenna is designed to match with the ground, that is matching between the antenna and the ground is perfect. In contrast, the matching between the antenna and air is not good. This is a main reason why the target below the asphalt layer is very difficult to trace.

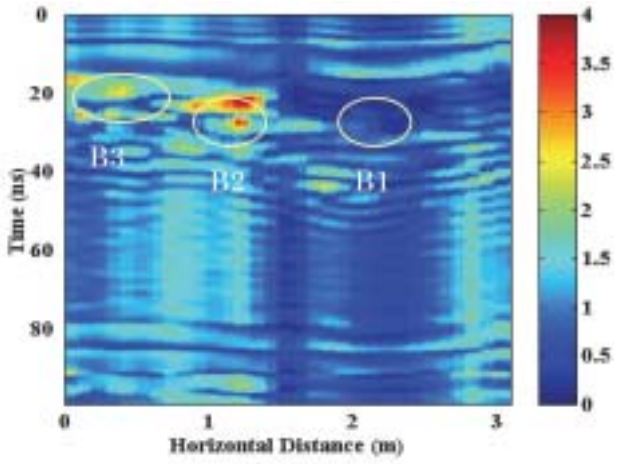

(a) The B-scan image processed by IFFT

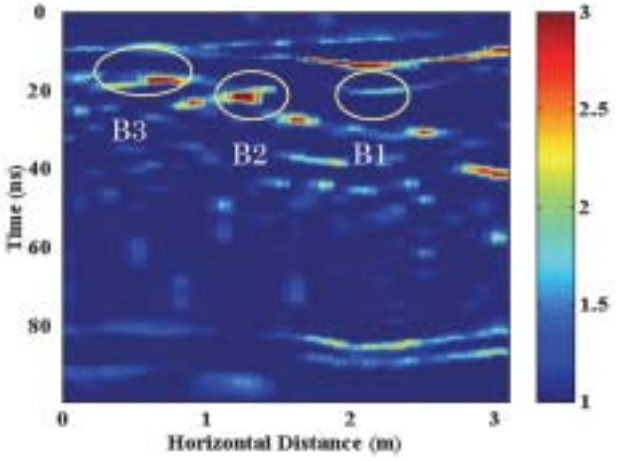

(b) The B-scan image processed by MUSIC

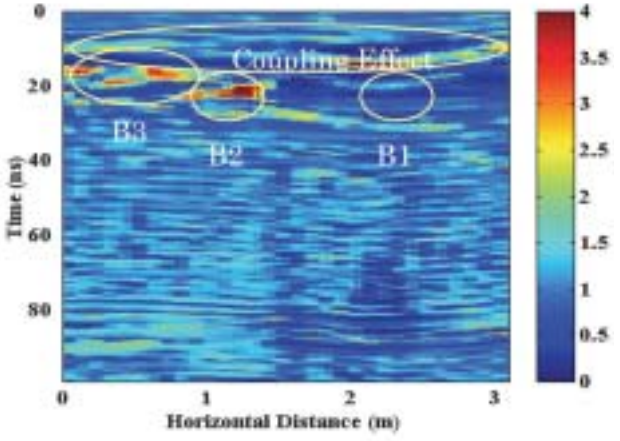

(c) The B-scan image processed by CPM

Plate 1 The B-scan images of buried pipe under the road pavement presented in linear scale. It was scanned on the gravel plus asphalt.

5.4 Three-Dimensional Imaging and Discussion

The B-scan image reconstructed from single scan is not good enough to figure out the pipe buried under the earth. However, if we scan the numbers of traces making an array of trace to get the 3-dimensional image or slice view using SAR method, the precise information about the underground target could be received. Therefore, 3-dimensional image and slice view is presented to give the precise information of the underground target. For that, the data was taken at the experiment field on the asphalt and the gravel as described in section 4.2. Scanning was performed up to 320 cm length at the interval of 10 cm in a trace. Again the antenna was shifted 10 cm right to scan another trace. Altogether five traces were scanned at an increment 10 cm. Therefore the total area scanned was 320 cm $\times$ 40 cm. Each trace was processed by IFFT, MUSIC, and CPM as in section 4.3 to get the B-scan image of the underground targets. The B-scan images thus obtained were arranged in an array to make two-dimensional (2-D) data. Then the two-dimensional data were further processed by SAR method. Here, we used migration technique to do SAR processing. The SAR processed results are presented in Plate 2, which is a time slice view. It is worthy to mention here that, relative permittivity (dielectric constant) is important while processing the migration technique. When the value of relative permittivity is varied the depth of target position seen in the slice view image in Plate 2 is also varied. Therefore, the correct value of relative permittivity is required for detecting the correct depth of the target.

The IFFT processed results were arranged in an array, which was further processed by SAR method and the results are presented in the Plate 2 (a) and (b). The resolution of the IFFT is not high, so the image reconstruction of the pile B3 and B2 are not prominent. Similarly, the MUSIC processed results were arranged in an array, which was further processed by SAR method and the results are presented in the Plate 2 (c) and (d). As the resolution of MUSIC is high, the slice images of pipe B3 and B2 are prominent and the continuity of pipes are also clearly visible. Checking the each B-scan traces processed by MUSIC, which is presented in the Plate 3, did thorough investigation. Each B-scan traces show the target position B2 and B3 at the similar position. Consequently, the slice image showed the continuity of target. However, we could not trace out target B1, as it was a plastic pipe. The three dimensional image of the target B3 and B2 is presented in Plate 4. The 3-D image could be rotated to see the target image from different angle and prospection. It is found that the pipe B3 is clearly seen and covers the entire length of the scanned traces. It looks almost like a cut piece of pipe. Pipe B2 also looks like pipe but could not demonstrate clear picture, as in the pipe B3.

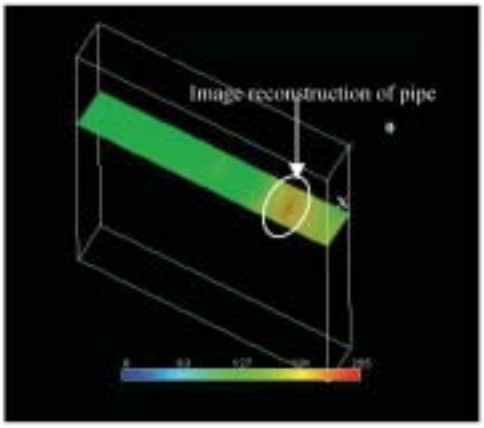

(a) Pipe B3 (Diameter=100mm) processed by IFFT

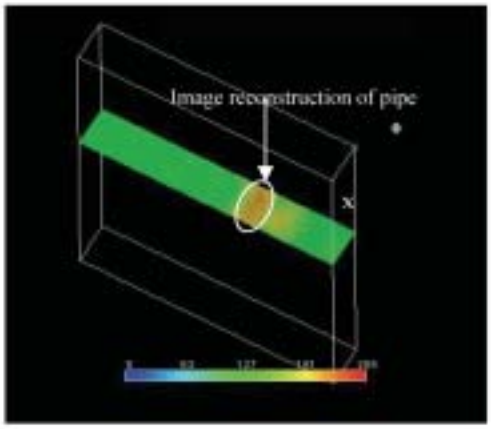

(b) Pipe B2 (Diameter=50 mm) processed by IFFT

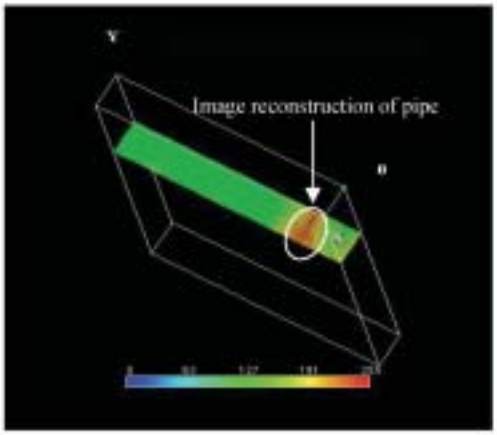

(c) Pipe B3 (Diameter=100mm) processed by MUSIC

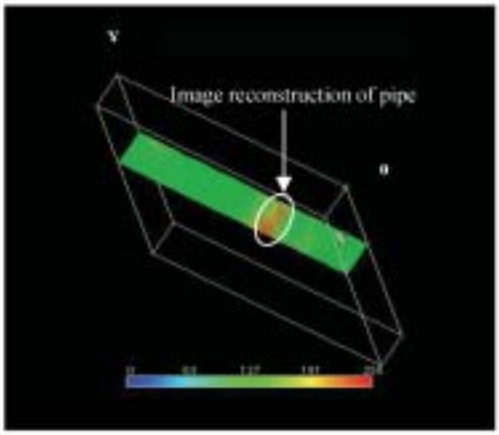

(d) Pipe B2 (Diameter=50mm) processed by MUSIC

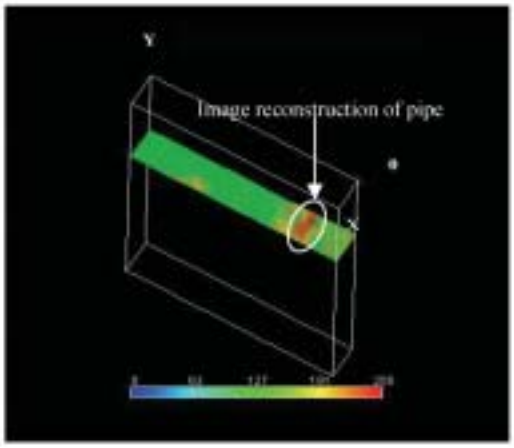

(e) Pipe B3 (Diameter=100mm) processed by CPM

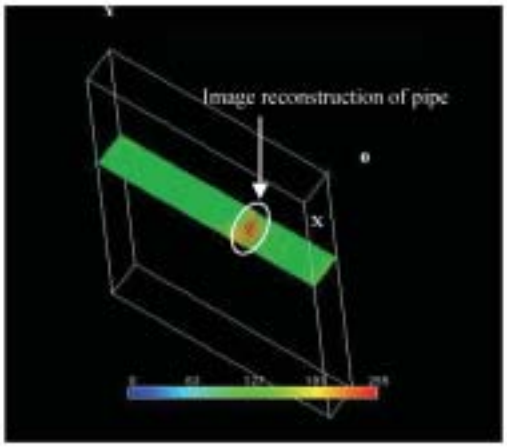

(f) Pipe B2 (Diameter=50mm) processed by CPM

Plate 2 Time slice view of the field experimental result of the buried pipe, which is processed by IFFT, MUSIC and CPM. The diameter of the pipe (metallic) was 100 mm and 50 mm respectively. Each trace is separated at the increment of 10 cm. The total area scanned was (40×320) cm. The travel time of each time slice view is about 21 ns (100 cm).

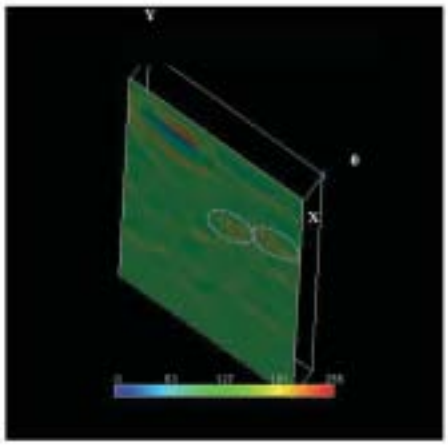

(a) B-scan image of initial trace

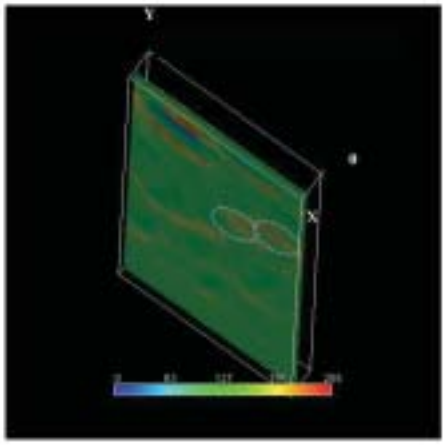

(b) B-scan image at 10 cm shifted from initial trace

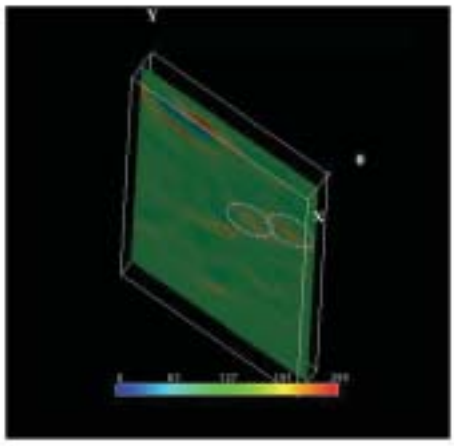

(c) B-scan image at 20 cm shifted from initial trace

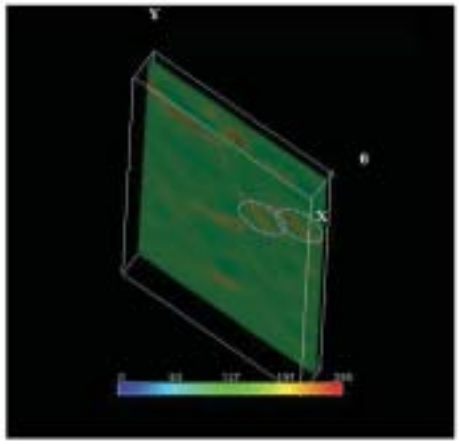

(d) B-scan image at 30 cm shifted from initial trace

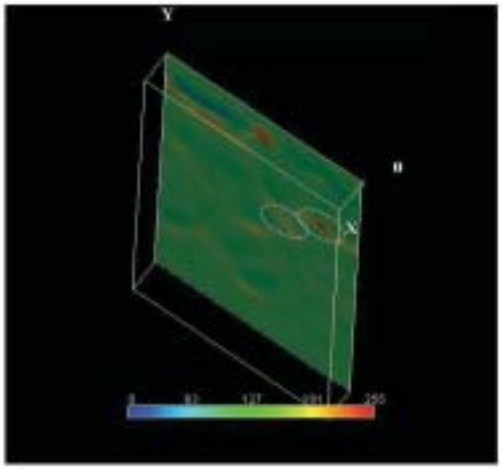

(e) B-scan image at 40cm shifted from initial trace

Plate 3 The scanning was performed for 3.2 cm length at the interval of 10 cm in a trace. Each trace is separated at the increment of 10 cm. The total area scanned was (40×320) cm. Each trace was processed by MUSIC to produce B-scan image and B-Scan result was further processed by SAR for 3-D representation.

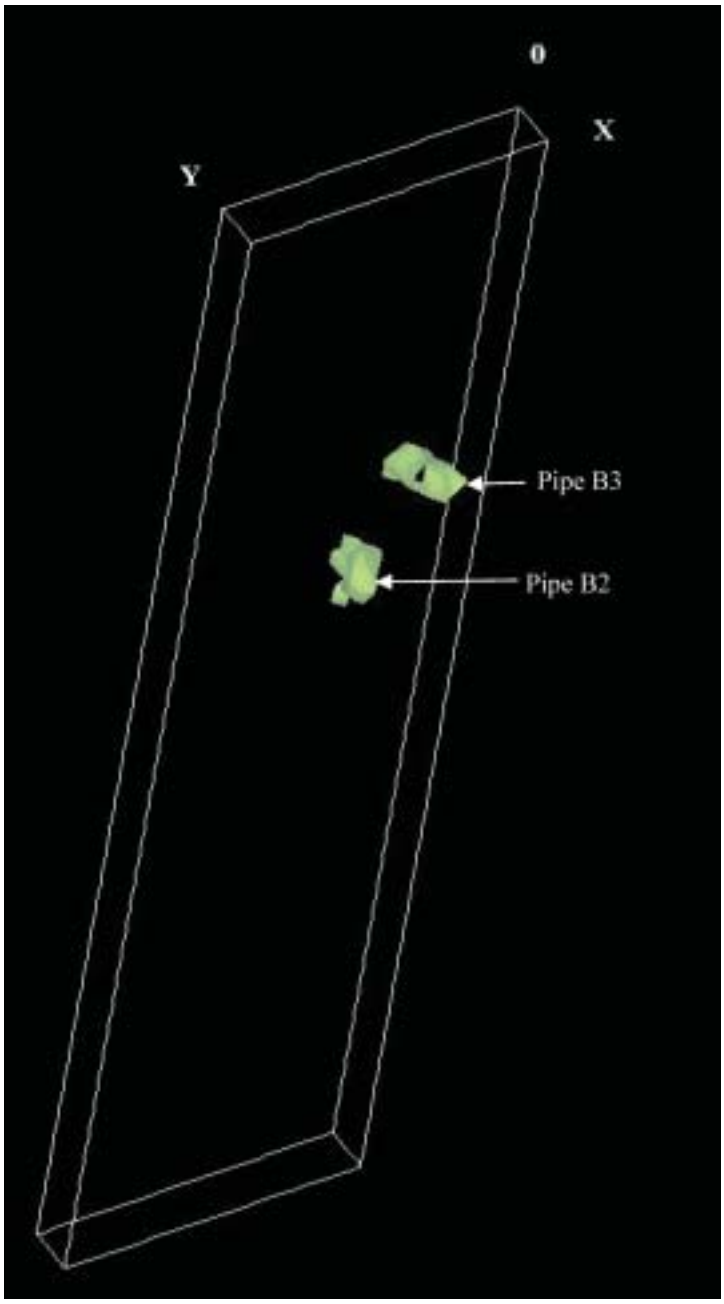

Plate 4 Three dimension image of Pipe B2 and B3. The one dimensional raw data was first processed by MUSIC to get B-scan image. The array of B-scan data (2-D data) was processed by SAR method.

Finally, the CPM processed results were arranged in an array, which was further processed by SAR method and the results are presented in the Plate 2 (e) and (f). As the resolution of CPM is also high due to the effect of MUSIC, the slice image of pipe B3 and B2 are very prominent and the continuity of pipes are also clearly visible. Checking the each B-scan traces processed by CPM as in previous case, which is presented in the Plate 5, also did thorough investigation. Each B-scan traces show the target position B2 and B3 at the similar position. Consequently, the slice image showed the continuity of target. The three dimensional image of the target B3 and B2 is presented in Plate 6. The 3-D image gives the clear information of the geometrical characteristic.

6. Conclusions

In this paper, we propose SFCW GPR with significantly improved signal processing algorithm for the civil engineering applications. Specifically speaking, we developed a high performance GPR model to detect underground gas pipes, water

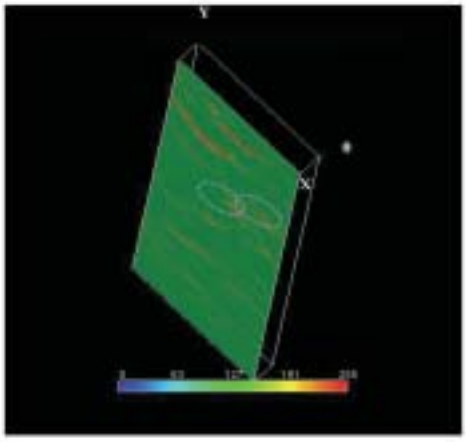

(a) B-scan image of initial trace

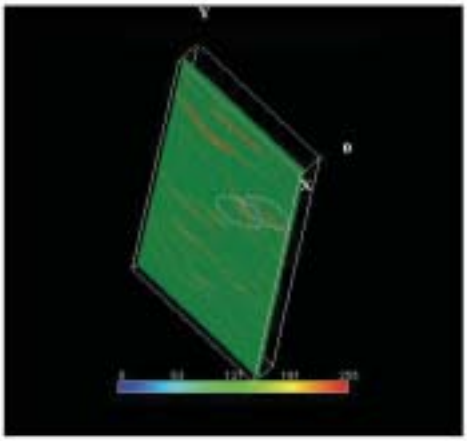

(b) B-scan image at 10 cm shifted from initial trace

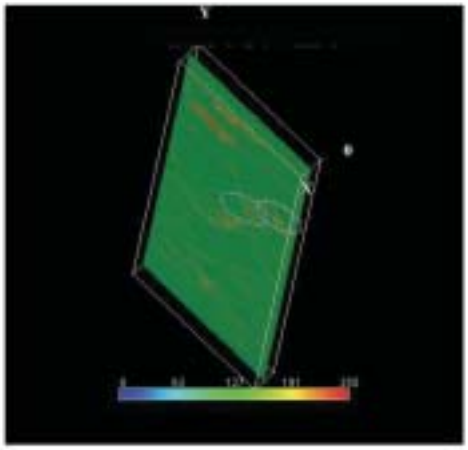

(c) B-scan image at 20 cm shifted from initial trace

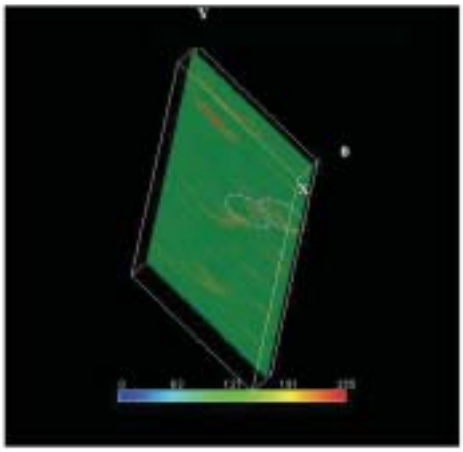

(d) B-scan image at 30 cm shifted from initial trace

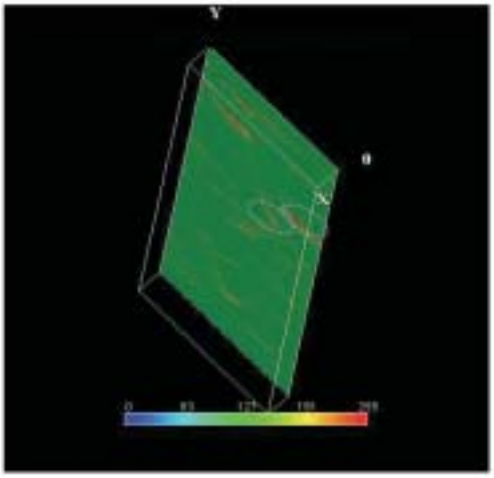

(e) B-scan image at 40cm shifted from initial trace

Plate 5 The scanning was performed for 3.2 cm length at the interval of 10 cm in a trace. Each trace is separated at the increment of 10 cm. The total area scanned was (40×320) cm. Each trace was processed by CPM to produce B-scan image and B-Scan result was further processed by SAR for 3-D representation.

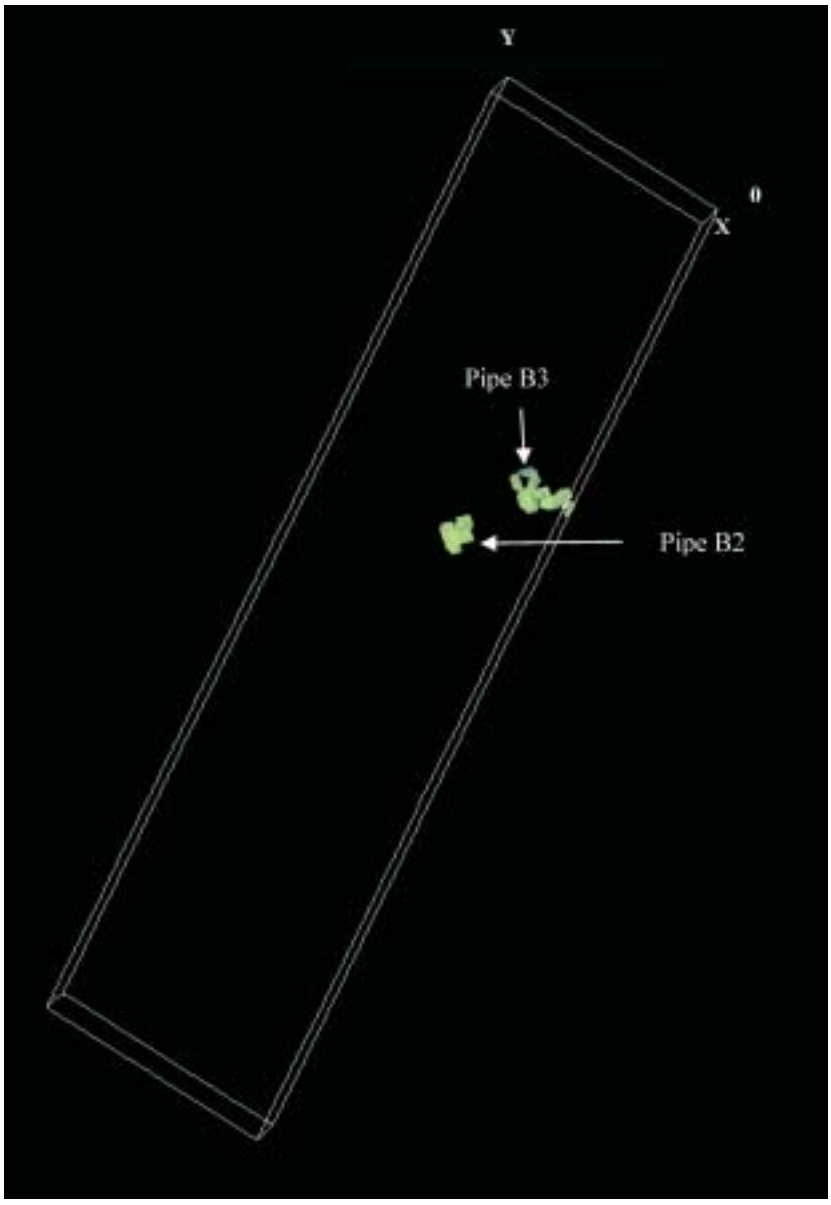

Plate 6 Three dimension image of Pipe B2 and B3. The one dimensional raw data was first processed by CPM to get B-scan image. The array of B-scan data (2-D data) was processed by SAR method.

pipes, electrical cables or ducts under the road layer, which are very important to detect before construction and maintenance of roads. We discuss the application of IFFT, MUSIC, and CPM signal processing algorithm in radar data to improve the vertical resolution and also to reconstruct the B-scan image of the buried targets. The CPM is a method of combining the time domain results of MUSIC and IFFT to achieve a good tradeoff between high resolution and a high precision signal level

In addition, application of SAR processing method has also been presented to improve the azimuth resolution and 3-D image reconstruction. A field experiment was performed on a gravel road and asphalt layer at a road construction company's test site in Saitama-shi, Japan. It is found from the signal processing results that CPM could reconstruct the B-scan image of pipes with high resolution. The SAR processing method was applied on an array B-Scan images of 2-D CPM data to obtain 3-D image of the targets. The 3-D image gives the clear information of the physical and geometrical characteristic of the buried pipes under a road.

Acknowledgements

The authors would like to express our gratitude to the

Nippo (Nippon Hodo Co. Ltd.), Saitama, Japan for creating test site for GPR experiment on a road. We would also like to acknowledge Mr. T. Nozu at the Koden-Electronics Company, Yamanashi Prefecture, Japan for his support in data acquisition.

References

1) X. Derobert, C. Faychard, P. Cote, E. L. Brusq, E. Guillanton, J. Y. Daungnac and C. Pichot : Step-frequency radar on thin road layers, Journal of Applied Geophysics Vol. 47, pp. 317–325, 2001.
2) D. Goodman : Ground-penetrating radar simulation in engineering and archaeology, Geophysics, Vol. 59, No. 2, pp. 224–232, 1994.
3) Y. Tomizawa and I. Arai : Subsurface Radar Using a Coded Signal without Time-sidelobes, Journal of Remote Sensing Society of Japan, Vol. 21, No. 5, pp. 423–430, 2001.
4) S. M. Shrestha, and I. Arai : Signal Processing of Ground Penetrating Radar Using Spectral Estimation Techniques to Estimate the Position of Buried Targets, EURASIP Journal on Applied Signal Processing, Vol. 2003, No. 12, pp. 1198–1209, 2003.
5) S. M. Shrestha, I. Arai and T. Miwa : Super Resolution Signal and Image Processing Technique for GPR Combining FFT and MUSIC Algorithms, Journal of The Remote Sensing Society of Japan, Vol. 23, No. 1, pp. 31–43, 2003.
6) W. R. Scott, Jr., J. S. Martin and G. D. Larson : Experimental Model for a Seismic Landmine Detection System : IEEE Trans. on Geoscience and Remote Sensing. Vol. 39, No. 6, 2001.
7) I. Arai and T. Suzuki : Experimental Results on Subsurface Radar with Improved Resolution : Journal of Electromagnetic Wave and Applications, Vol. 7, No. 11, pp. 1479–1495, 1993.
8) T. Yamakura, H. Yamada and Y. Yamaguchi : Resolution Improvement of the MUSIC Algorithm Utilizing Two Different Polarized Antenna, IEICE Trans. Commun., Vol. E79-B, No. 12, pp. 1827–1832, 1996.
9) I. Arai, Y. Tomizawa and M. Hirose : Pulse Compression Subsurface Radar, IEICE Trans. Commun., Vol. E83-B, No. 1, 2000.
10) J. E. Evans, J. R. Johnson and D. F. Sun : Application of advanced signal processing techniques to angle of arrival estimation in ATC navigation and surveillance systems, M.I. T. Lincon Lab., Lexington, MA, Tech. Rep. 582, 1982.
11) R. O. Schmidt : Multiple Emitter Location and Signal Parameter Estimation, IEEE Trans. Antenna Propagations, Vol. AP-34, pp. 553–1560, 1986.
12) R. T. Williams, S. Prasad, A. K. Mahalanabis and L. H. Sibul : An Improved Spatial Smoothing Technique for Bearing Estimation in a Multipath Environment, IEEE Trans. on Acoustics, speech, and signal processing. Vol. ASSP-36, No. 4, 1988.
13) T. Shan, M. Wax and T. Kailath : On Spatial Smoothing for Direction-of Arrival Estimation of Coherent Signals, IEEE Trans. on Acoustics, speech, and signal processing. Vol. ASSP-33, No. 4, 1985.
14) H. Yamada, M. Ohmiya and Y. Ogawa : Super Resolution Techniques for Time-Domain Measurements with a Network Analyzer, IEEE Trans. on Antennas and propagation. Vol. 39, No. 2, 1991.
15) Y. Ogawa and N. Kikuma : High-Resolution Techniques in Signal Processing Antennas, IEICE Trans. on Commun., Vol. E78-B, No. 11, pp. 1435–1441, 1995.
16) A. Yoshizawa and T. Iwasaki : Image Reconstruction in Optical Frequency-Domain Reflectometry by means of Maximum Entropy Method — Fourier Transform Combination, IEICE Trans., Vol. J76-C-I, No. 6, pp. 215–221, 1993.
17) R. Roy and T. Kailath : ESPRIT — Estimation of Signal Parameters Via Rotational Invariance Techniques, IEEE Trans. on Acoustics, Speech and Signal Processing, Vol. 37, No. 7, pp. 984–994, 1989.
18) J. I. Halman, K. A. Shubert and G. T. Ruck : SAR Processing of Ground-Penetrating Radar Data for Buried UXO Detection : Results from a Surface-Based System, IEEE Trans. on Antennas and Propagation, Vol. 46, No. 7, pp. 1023–1027, 1998.
19) I. Arai and T. Suzuki : Subsurface Radar (Part 2) —Compression Type—, IEICE Technical Report. Vol. SANE83–8, 1983.
20) I. Arai and T. Suzuki : Synthetic Aperture for Subsurface Radar, Proc. of ISAP '85, pp. 655–658, 152–1, 1985.
21) S. Valle, L. Zanzi, M. Sgheiz, G. Lenzi and J. Friborg : Ground Penetrating Radar Antennas : Theoretical and Experimental Directivity Functions, IEEE Trans. on Geoscience and Remote Sensing, Vol. 39, No. 4, pp. 749–759, 2001.
22) C. Dourthe, C. Pichot, J. Dauvignac and L. Balanc-Feraud : Regularized Bi-Conjugate Gradient Algorithm for Tomographic Reconstruction of Buried Objects, IEICE Trans. on Electron, Vol. E83-C, No. 12, pp. 1858–1863, 2000.
23) M. I. Skolnik : Radar Handbook, Second Edition, McGraw-Hill, 1990.
24) S. M. Shrestha, I. Arai, T. Miwa and Y. Tomizawa : Signal Processing of Ground Penetrating Radar Using Super Resolution Technique, IEEE Proc., 2001 IEEE Radar Conference, Atlanta, Georgia, pp. 300–305, 2001.
25) K. Kim, D. Seo and H. Kim : Efficient Radar Target Recognition Using the MUSIC Algorithm and Invariant Features, IEEE Trans. on Antennas and propagation. Vol. 50, No. 3, 2002.
26) S. M. Shrestha, I. Arai and T. Miwa : Application Possibilities of Super Resolution Technique For GPR Imaging, Proc. of SPIE, Vol.4785, Ninth International Conference on GPR, Santa Barbara, USA, pp. 508–513, 2002.
27) S. M. Shrestha and I. Arai : High Resolution Image Reconstruction by GPR using MUSIC and SAR Processing Method for Landmine Detection, Proc. IEEE Geoscience and Remote Sensing Soc. Int. Symp., IGARSS 2003, Toulouse, France, 2003.

28）Y. Ogawa, N. Hamaguchi, K. Ohshima and K. Itoh : High-Resolution Analysis of Indoor Multipath Propagation Structure, IEEE Trans. Commun., Vol. E78-B, No. 11, pp. 1450–1457, 1995.

〔著者紹介〕

●**Shanker Man Shrestha（シャンカー　マン　シュレスタ）**

1967年5月生。’93年バングラディッシュ技術工科大学（BUET）電気電子工学科卒。’94年～’97年Nepal Telecommunications Corporation（NTC）電信技術計画課，’97年～’98年同社衛星通信サガルマタ地球局勤務。’98年～’99年電気通信大学研究生。’01年同大電気通信学研究科電子工学専攻修士課程修了，’04年同大大学院博士課程了。’04　年明星電気株式会社を経て，’07年　シュルンベルジェ株式会社，現在に至る。工博。ディジタル信号処理，レーダ画像処理，地中探査レーダ，超分解能信号処理の研究に従事。日本リモートセンシング学会，IEEE学会員。

E-mail : SShrestha2@slb.com

●**富澤　良行（トミザワ　ヨシユキ）**

1964年3月生。’86年電気通信大学応用電子工学科卒，’88年同大大学院修士課程修了。’90年群馬高専電気工学科助手などを経て，’07同高専電子メディア工学科准教授，現在に至る。工博。地中探査レーダなど電磁波計測の研究に従事。日本リモートセンシング学会，電子情報通信学会会員。

E-mail : tomizawa@elc.gunma-ct.ac.jp

●**荒井　郁男（アライ　イクオ）**

1941年6月生。’65年電気通信大学電波通信学科海上通信専攻卒，’67年同大大学院修士課程修了。’67年同大電気通信学部助手などを経て，’94年同大電子工学科教授。工博。主として地中レーダ，マイクロ波リモートセンシング，マイクロ波による生体計測に関する研究に従事。日本リモートセンシング学会，電子情報通信学会フェロー。